Position Estimation Using Linear Hall Sensors for Permanent Magnet Linear Motor Systems

Jonghwa Kim, *Student Member, IEEE*, Seibum Choi, *Member, IEEE*, Kwanghyun Cho, *Member, IEEE*, and Kanghyun Nam, *Member, IEEE*

***Abstract*—This paper proposes a new scaleless position estimation method. From the industrial perspective, the Hall sensor has several advantages: tiny size, light weight, extremely low cost, and insensitivity to environmental contamination and external disturbance. Compared to the square wave Hall sensor, the linear Hall sensor provides more detailed information along the position. However, for combining more than two linear Hall sensors, the sensor offset, the difference in scale, and the unwanted phase shift between them and the harmonics would decrease the validity and reliability of sensor measurement. The fast Fourier transform and the fixed point iteration method are applied to compensate for those issues without any low-pass filter or additional signal conditioning. The effectiveness of the proposed scheme is verified through a prototype permanent magnet linear synchronous motor system.**

***Index Terms*—Fast Fourier transform (FFT), fixed point iteration method, initial position alignment, linear Hall sensor, Newton method, permanent magnet linear motor, position estimation, scaleless motor system.**

I. Introduction

DUE to increasing demand and development in industrial technology, the importance of accurate and precise motion control has been highlighted for decades. Although there are some other components that affect the performance of motion control, such as sampling time, system bandwidth, control strategy, sensitivity to circumstances, and physical conformation, one of the most influential sources is the sensor. Unlike the constant V/f control that considers only the average torque, the exact rotor position information is essential for the vector control in which the magnitude and phase of armature current must be adjusted according to the rotor position to accomplish instantaneous torque control.

The two most widely used typical sensors for position measurement are the encoder [1], [2] and the resolver [3], [4]. The optical incremental encoder exhibits outstanding performance in resolution. However, the header (reader) and the scale are still high priced, and the cost increases with the required stroke due to an additional scale. The sensitivity to contamination and environment such as oil, moisture, dust, obstacle, vibration, and shock limits its industrial applicability. In the case of the resolver, although the durability and the reliability are achievable through its sturdy hardware, its considerable size and weight remain an issue.

In the 1990s, Matsui suggested a speed and position sensorless control method by formulating the position estimation error in the back electromotive force term of the current and voltage model [5]. Many similar and improved studies have been conducted until recently [6]–[11]: orthogonal permanent magnet flux observer [7], D-state observer [8], tap voltage utilization [9], signal injection [10], and online parameter identification [11]. However, those methods require exact model parameters and are sensitive to the time-varying components and unexpected disturbances. In the electric motor dynamics, the variables and coefficients generally vary with temperature, load, and velocity, among others. As a representative example, the coil temperature of an electric washing machine for household purposes rises from 30 °C to 110 °C under a full load in just 10 min, and this leads to an increase of 30% in coil resistance [12]. The d-axis and q-axis inductances calculated in the rotor reference frame are not even constant in a linear motor system due to nonuniform permanent magnets along the rail. The voltage, not measured in general, is brought from the desired value of the current controller output, which is not identical to the real voltage at the load change timing [13] or at the commutation point of the pulse width modulation (PWM) inverter [14]. The starting procedure in a sensorless scheme is another issue [15], [16].

The Hall effect sensor has been studied as a scaleless position estimator for its independent properties to coil inductance and resistance. By attaching two square wave Hall sensors 90 electrical degrees apart, rising or falling edge signals at every 90 electrical degrees are obtainable. This kind of estimator does not diverge, but the resolution is low and the pulse intervals are not equal along the position in a linear motor system. Therefore, the velocity calculated through counting the time interval between adjacent pulses provides only approximate information even under constant speed operating conditions, and it gets worse at

Manuscript received January 4, 2016; revised April 25, 2016; accepted June 3, 2016. Date of publication July 18, 2016; date of current version November 8, 2016. This work was supported in part by the Ministry of Science, ICT and Future Planning (MSIP), Korea, under the Information Technology Research Center support program (IITP-2016-H8601-16-1005) supervised by the Institute for Information and Communications Technology Promotion, the BK21 plus program, and the Technological Innovation R&D program of SMBA (S2341501), and in part by a National Research Foundation of Korea grant funded by the Korea government (MSIP) under Grant 2010-0028680. *(Corresponding author: Seibum Choi.)*

J. Kim and S. Choi are with the Department of Mechanical Engineering, Korea Advanced Institute of Science and Technology, Daejeon 34141, South Korea (e-mail: jjong52@kaist.ac.kr; sbchoi@kaist.ac.kr).

K. Cho is with Samsung Electronics, Hwaseong-si 445-330, South Korea (e-mail: khcho0960@gmail.com).

K. Nam is with the School of Mechanical Engineering, Yeungnam University, Gyeongsan, 38541, South Korea (e-mail: khnam@yu.ac.kr).

Color versions of one or more of the figures in this letter are available online at http://ieeexplore.ieee.org.

Digital Object Identifier 10.1109/TIE.2016.2591899

0278-0046 © 2016 IEEE. Personal use is permitted, but republication/redistribution requires IEEE permission.
See http://www.ieee.org/publications_standards/publications/rights/index.html for more information.

low speed or velocity varying conditions and at load changing timing [17]. Although multiple Hall sensor installation leads to a finer resolution, e.g., 60 electrical degrees of resolution with three Hall sensors [18], there is a spatial constraint in general. Meanwhile, to prevent detecting a noise as an edge signal erroneously, a combination of Hall sensor states of multiple sensors, e.g., (1, 0, 0) for three Hall sensors, was used to estimate velocity in [19]. The maximum time error in that method could amount up to two times of the sampling time, and the influence of this error to the estimated value will increase at a higher traveling speed. With multiple sensor installation, an alignment error also aggravates the estimated result. To compensate this error, some studies were conducted: signal analysis at a compulsory constant speed by an additional dynamometer [20], an averaging method [21], and a dual flux observer [22].

Some fusion methods have been suggested. In [18], the sensorless method and square wave Hall sensors were combined. However, high and constant speed conditions were necessary for that scheme to cancel out the voltage drop by coil resistance (IR) and current differentiation. The vector tracking observer and three square wave Hall sensors were utilized in [13] and [23]. The optimal intersensor weighting calculation approach through the radial basis function between a magnetic encoder with 2 mm resolution and an analog velocity sensor was adopted in [24]. Conjunction of an accelerometer and three Hall sensors was studied in [25].

Since the 2000s, the linear Hall sensor has been receiving attention for its finer resolution than that of the square wave Hall sensor signal [14], [26]–[30]. The position information in the form of angle (radian) can be obtained through arctan calculation if ideal sine and cosine signals are measured by two linear Hall sensors that are 90 electrical degrees apart. To make the raw signal an ideal sinusoidal waveform, nonideal components such as the sensor offset and the scale difference between sensors and the unwanted phase shift due to an alignment error should be compensated by adequate signal conditioning [14], [27], [29]. However, those methods were designed and verified for rotary motor systems in which the nonideal components show the characteristic of periodicity, but this does not occur in the linear motor system. For example, in [14], the offset was compensated by averaging the previous period data. However, in the linear motor system, the signal offset and scale change along the position because of nonuniform permanent magnets on the rail as well as the sensor itself. Furthermore, as reported in some studies [7], [9], [27]–[30], the magnetic flux distribution in the air-gap magnetic field has some kind of harmonics. Considering the number of harmonics, 2^n Hall sensors for the nth-order harmonics [27] or adaptive notch filter design for each target harmonics [28] are not efficient approaches. Furthermore, reshaping the permanent magnets to optimized shapes [29] or the Halbach magnet array [30], [31] is not a general solution.

In this study, a sensor signal modeling through fast Fourier transform (FFT) analysis and position estimator design using a fixed point iteration method are presented to overcome the above weaknesses and limitations.

The rest of this paper is organized as follows. Sections II–IV discuss the Hall sensor characteristics, Hall sensor signal modeling, and position estimator design, respectively. Section V gives a convergence proof, and a comparative study is conducted in Section VI. A conclusion is made in Section VII.

TABLE I
COMPARISON OF SENSOR PROPERTIES

	Optical encoder	Resolver	Hall sensor
Sensitivity to shock	High	Low	Low
Sensitivity to vibration	High	Low	Low
Sensitivity to oil, dust	High	Low	Low
Size	Big	Big	Very small
Weight	Medium	Heavy	Very light
Resolution	Extremely high	High	Low
Necessity of scale	Yes	No	No
Price	Very expensive	Medium	Very cheap

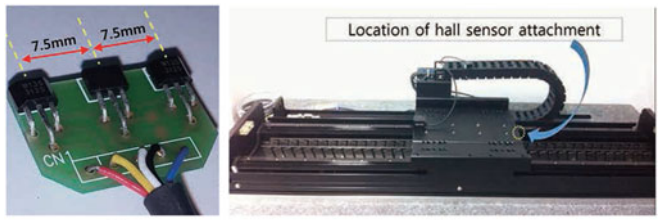

Fig. 1. Hall sensor array on (a) PCB and (b) applied linear motor system.

II. HALL SENSOR CHARACTERISTICS

The Hall sensor utilizes the Hall effect, which is the voltage difference across an electrical conductor, transverse to an electric current in the conductor and a magnetic field perpendicular to the current. Since the magnetic field is robust to external physicochemical factors and the structure of the Hall sensor is simple, the Hall sensor has competitive properties as a position detection sensor. A comparison of the Hall sensor with the encoder and resolver is presented in Table I.

The Hall sensor used in this work was WSH136 by Winson Semiconductor Corporation. Three Hall sensors were one-dimensional arrayed with intervals of 120 electrical degrees. Although the pole pitch of the applied linear motor system was 22.5 mm (i.e., 45 mm for 360 electrical degrees and 30 mm for 240 electrical degrees), the entire length of the sensor array was only 15 mm by attaching the middle Hall sensor in the reverse direction to the others, as shown in Fig. 1(a). The location of the sensor attachment and the applied prototype linear motor system is shown in Fig. 1(b). The system parameters are given in Table II. These parameters were obtained by a system identification method, which is not described in this paper. The PWM inverter used for the experiments had a switching frequency of 10 kHz and was controlled by dSPACE DS-1103. The current and position controls were executed at 50 μs and 0.5 ms loop times, respectively. An optical linear encoder, which had a resolution of 0.5 μm, was installed to measure the true

TABLE II
PARAMETERS OF THE HALL SENSOR AND PMLSM SYSTEM

Parameter	Value	Unit
Mover mass	6.70	kg
Viscous friction coefficient	57.7	N/m/s
Pole pitch	22.5	mm
Sensitivity	3.0	mV/G
Measurable gauss range	±1500	Gauss
Temperature drift	±0.3	mV/°C

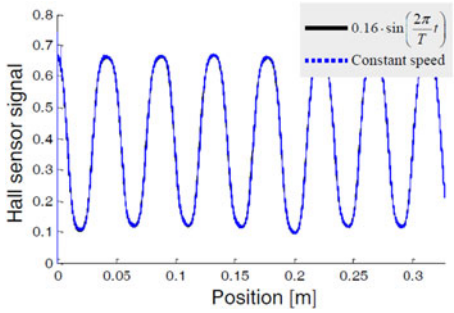

Fig. 2. Hall sensor signal at identical position with different travel speeds. (Black solid line: sinusoidal position trajectory with period T of 1, 2, 4, 6, and 8 s, and 0.32 m stroke, blue dotted line: constant speed of 0.02, 0.06, 0.10, 0.15, and 0.20 m/s.)

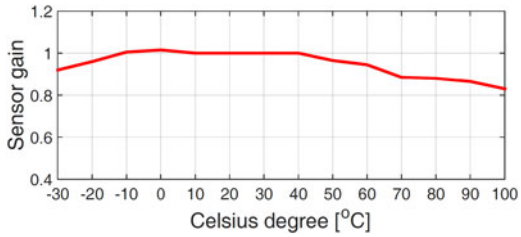

Fig. 3. Hall sensor drift on temperature.

position for the performance validation and initial Hall sensor signal modeling.

The essential position dependent characteristic of the Hall sensor signal as a position detector was first verified, as shown in Fig. 2. As mentioned below, the line overlaps with various traveling conditions, of which the maximum instantaneous velocity exceeds 1 m/s. The black solid lines indicate five cases of a sinusoidal reference trajectory and the blue dotted lines show five cases of constant speed. However, the black solid lines are almost invisible since they are overlapped by the blue dotted lines. This result confirms that the Hall sensor signal is position dependent and velocity independent. Using this property, in the following section, sensor signal modeling for positioning is conducted through FFT of the position signal.

Another property that is of concern is the temperature-dependent signal drift. The data sheet, provided by the manufacturer, shows that the sensitivity versus temperature graph is almost flat between 5 °C and 40 °C, as shown in Fig. 3.

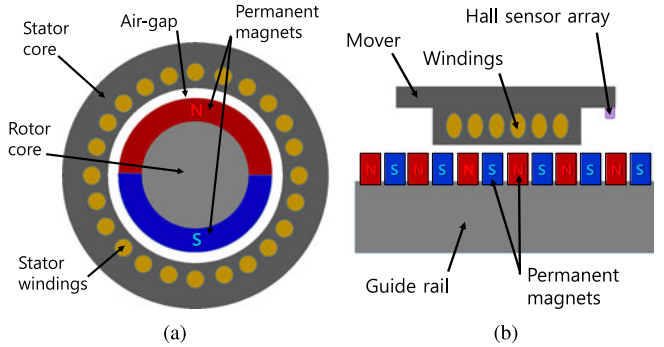

Fig. 4. Simplified general motor structure of (a) rotary type motor and (b) linear motor.

There are some geometrical advantages of a linear motor system over a rotary motor system. As depicted in Fig. 4(a), in a rotary motor system, the Hall sensor should be installed in the air gap between the stator and the rotor. Therefore, the Hall sensor measurement is affected by the armature reaction (i.e., the Hall sensor senses the magnetic flux induced by not only the permanent magnets, but also the current flowing in the armature coil). This narrow and closed structure of the air gap is adverse to heat radiation, which influences the Hall sensor sensitivity and the magnetic flux density itself of permanent magnets. On the other hand, in a linear motor system, the Hall sensor can be attached at the open space apart from the coil but still near the permanent magnets, as shown in Fig. 4(b). This leads to the design that is free from the effect of armature reaction in the Hall sensor measurement and has good thermal radiation as well. Therefore, the temperature during normal operation is expected not to exceed 40 °C. It should be noted that the armature reaction also affects the magnetic flux distribution in the air gap between the permanent magnet and armature coil in linear motor systems [32], even though sometimes it is not considered in some analytical methods [33]. Nevertheless, the Hall sensor measurement is not affected by the armature reaction for the mover shaped as shown in Fig. 4(b), that is, the shape widely used in linear motor systems [34].

From the structural characteristics of linear motor systems, the number of permanent magnets increases proportionally to the required operating range, and variations are inevitable in the magnetic flux density among the magnets. Also sensor offsets, difference in sensor scales, and unexpected phase shift in arrayed sensors are inevitable. Meanwhile, as described in the previous section, the magnetic flux distribution to the position is not quite an ideal sinusoidal wave and is actually composed of several harmonics.

III. HALL SENSOR SIGNAL MODELING

In this section, the issues mentioned above are solved by modeling the variations in a lumped form through offline FFT analysis along the position, which has three main advantages. First, it can be modeled using only a few parameters. Second, since the high-frequency noise term in Hall sensor measurement is distinguishable from the Hall sensor signal, an additional

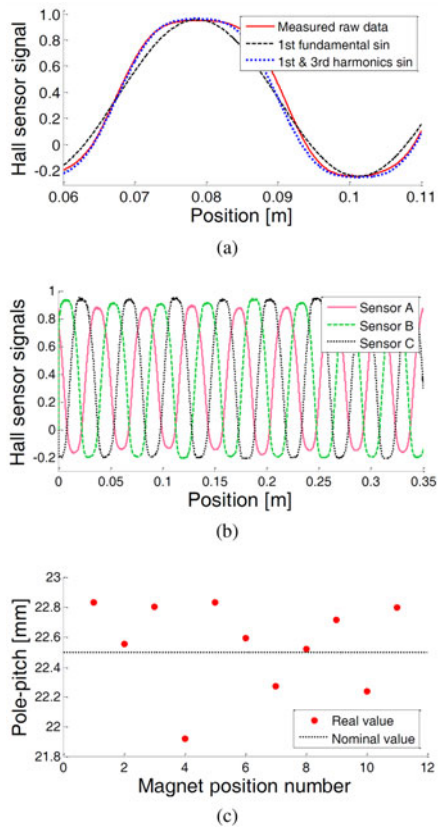

Fig. 5. Hall sensor measurement analysis with (a) harmonics components, (b) differences in sensor offset, scale, and unwanted phase between arrayed sensors, and (c) unequal pole pitches.

low-pass filter is not necessary to filter out noise that causes a phase lag. Third, since the Hall sensor is insensitive to other factors, there is no need for an online adaptation algorithm to update the model. Actually, the initial offline modeling can be regarded as a part of sensor calibration that should be done at least once for initial setting and periodically for maintenance.

Raw Hall sensor signals are first analyzed, as shown in Fig. 5: (a) describes the harmonics existence in a sensor measurement in comparison with a sine function of fundamental harmonics and also after combination with the third-order harmonics; (b) represents the difference in scale, offset, and the unwanted phase shift between the arrayed three sensor signals; and (c) indicates nonidentical pole pitches.

As mentioned earlier and can easily be seen in Fig. 5(a), there exist several harmonics in the Hall sensor measurement. Through FFT analysis, the magnetic field of permanent magnets along the position is modeled as the summation of harmonic functions. The magnitudes of all harmonics calculated through a trigonometric formula are summarized in Table III. Even though the fundamental and the third-order harmonics are dominant, there are still some other harmonics with considerable amounts. It should be noted that the dominating third-order harmonic component in flux distribution from the permanent magnet is due to the arrangement pattern of the magnetic array. Due to the symmetric nature of the magnetic array along the direction of motion, the odd number harmonics are dominant. In addition,

TABLE III
NORMALIZED MAGNITUDE OF EACH HARMONIC

Harmonics	Normalized magnitude	Model "P" inclusion	Model "AP" inclusion
1st	100%	√	√
2nd	3.9%	√	√
3rd	9.9%	√	√
4th	2.7%	√	√
2/7th	1.5%	√	√
3/7th	1.0%		√
10/7th	1.0%		√
11/7th	1.1%		√

[1]First harmonic represents the fundamental harmonic of 45-mm pole pair.
[2]Fractional harmonics are induced for intermagnet unequal properties, and 2/7th harmonics means 2/7 times of the fundamental harmonic.

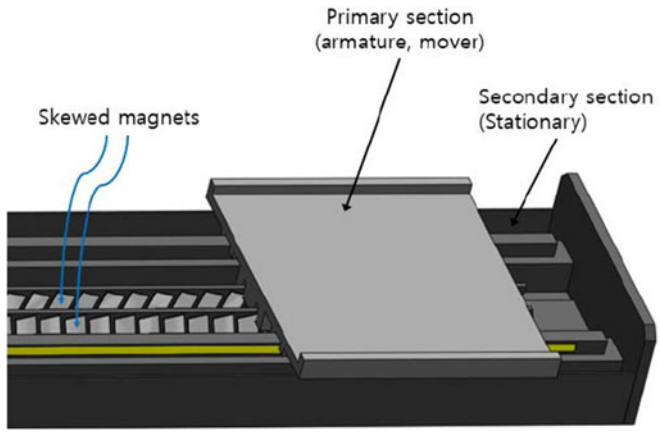

Fig. 6. Skewed permanent magnets.

one more expected reason is that the permanent magnets are skewed as shown in Fig. 6, for the sake of detent force reduction.

Two Hall sensor signal models are defined as Model "P" and Model "AP" using different numbers of sinusoidal harmonic functions. As summarized in Table III and described below, Model "P" mainly consists of periodic components of the 1st-order to the 4th-order harmonics, and the 2/7th-order harmonic component is included in order to reflect aperiodicity in magnetic flux distribution along the magnets. For more consideration of the aperiodicity, additional 3/7th-, 10/7th-, and 11/7th-order harmonic components are included in Model "AP."

IV. POSITION ESTIMATOR DESIGN

In Fig. 5(b), only the regions where the signal slope is large enough are used for the position estimation. That means that only one sensor signal is used at a time for the following considerations. First, the effects of unequal properties between the pole pairs stand out more near the signal peaks. Second, the modeling error using the limited number of harmonics is more dominant near the peaks. Third, position estimation accuracy is increased proportionally to the stiffness of the signal slope, especially considering the measurement noise. Finally, with the

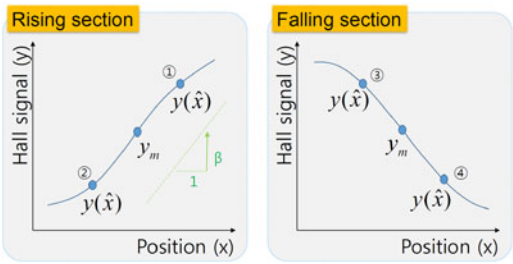

Fig. 7. Sensor signal model decomposition into two sections.

signal near the peak, it is very difficult to recognize the change of direction. Therefore, out of three signals, one signal that is nearest to the magnetic neutral point, i.e., around 0.4 in Fig. 5(b), is selected.

The Hall sensor signal model y described in the previous section can be expressed with several harmonic components as follows:

$$y(x) = A_0 + \sum_k A_k \sin(kx + B_k) \tag{1}$$

where A_0 is the dc component, k is the harmonic number, A_k is the magnitude of harmonic component for harmonic number k, x is the position, and B_k is the phase of the harmonic component for harmonic number k. Since the model consists of sinusoidal functions, it cannot be inverted to get the position information directly from the sensor measurement. Also for harmonics functions, there can exist multiple input candidates for the same measurement output. Therefore, a unique and correct solution (position) is not directly extracted from a measurement. Instead, an iterative estimation method is suggested. The sensor signal model at the region of interest is decomposed into rising and falling sections, as shown in Fig. 7. The position estimator algorithm runs as follows:

$$\hat{x}_n = \hat{x}_{n-1} + \frac{1}{\beta}\{y_m - y(\hat{x}_{n-1})\} \tag{2}$$

where $\hat{x}_n$ is the estimated position at step n, y_m is the Hall sensor measurement, and β is the inclination angle of the signal model around the estimated position. In the cases of ① or ② in Fig. 7 (i.e., the rising section), β has a positive value, and in the cases of ③ or ④, β becomes negative. Currently, the sampling times for both the position estimation and measurement update are set identical to that of the mechanical position controller. However, the estimation loop can be run ten times faster without severe computational burden since the electric current control loop is already running at that speed with no problem. Also, the absolute magnitude of β is considered as a constant, which seems reasonable for the region of in Fig. 5(b) and is also confirmed by numerical validation, which is omitted here.

The performance of the position estimation method described in (2) is analyzed as follows. In Fig. 8, the position estimation error is plotted for several different speed conditions, as shown in Fig. 2. Since Model "AP" reflects the aperiodicity along the magnets, the estimation result shows less estimation error and less position dependence along the position compared to the

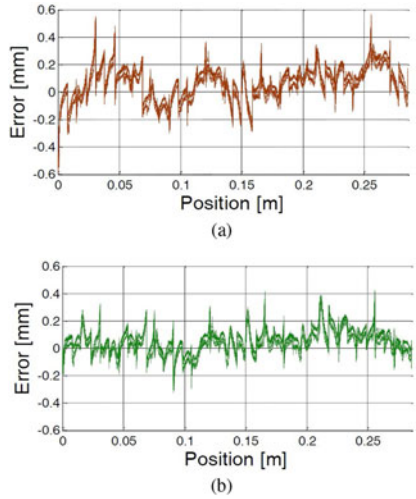

Fig. 8. Position estimation error with the suggested method of (a) Model "P" and (b) Model "AP."

TABLE IV
MAX AND RMS POSITION ESTIMATION ERROR

	RMS error		Max error	
	[mm]	[°E][1)]	[mm]	[°E]
Model "P"	0.1232	0.9856	0.4844	3.8752
Model "AP"	0.0953	0.7624	0.3649	2.9192

[1]Electrical degree.

result of Model "P." The difference in the performance between models "P" and "AP" can get smaller in case the aperiodicity is reduced with more advanced hardware. In Table IV, the RMS error and maximum error of both the models are summarized. For a reference, the unit in electrical degrees is more meaningful because the value in mm units changes according to the pole pair. (That is, with a shorter pole pair than 45 mm used in this study, the error in mm units would be smaller.)

One remaining problem with this method is that in the case of an extremely high traveling speed, the traveling distance can pass one pole pair distance during one sampling time. Therefore, there is a maximum speed limit with the proposed scheme, but the limit can be expanded easily with a shorter sampling time and a longer pole pitch. In this study, it reaches 90 m/s with a 45-mm pole pair and 0.5 ms sampling time.

V. CONVERGENCE PROOF

The convergence property of the iterative method suggested in (2) is verified by the following two similar but different approaches.

A. Newton–Raphson Method

The Newton method aims to find the approximate solutions of an equation $f(x) = 0$ by the iterative numerical method as follows:

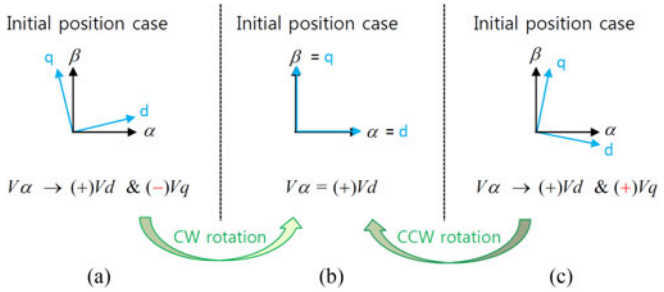

Fig. 9. Initial position aligning mechanism by applying V_α.

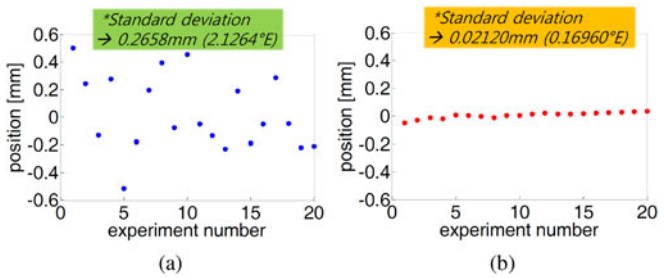

Fig. 10. Experimental verification of the initial position aligning method: (a) aligned by eye and (b) aligned by V_{alpha} application.

$$\hat{x}_n = \hat{x}_{n-1} - \frac{f(\hat{x}_{n-1})}{f'(\hat{x}_{n-1})} \tag{3}$$

where the prime means the differentiation with respect to position. By letting $f(\hat{x}) = y(\hat{x}) - y_m$, (2) is easily transformed into (3). The convergence theorem for the Newton method is given below.

Theorem V.1: Let f be a twice continuously differentiable function on the interval $[a, b]$ with $p \in (a, b)$ and $f(p) = 0$. Further suppose that $f'(p) \neq 0$. Then there exists a $\delta > 0$ such that for any $p_0 \in I = [p - \delta, p + \delta]$, the sequence $\{p_n\}$ generated by Newton's method converges to p.

Theorem V.1 can be interpreted as follows.

1) x_0 should be chosen sufficiently close to the root.
2) $f'(x)$ should not be too small near the solution.
3) $f''(x)$ should not be too large.

The second and third points above can be assured by the constant β in (2) for the $f'(x)$. For the first point, the initial starting point aligning method is applied.

1) Initial Position Alignment Method: For successful vector control in permanent magnet motor systems, the mover should be initially settled at the ideal "zero" position, where the d-axis in the synchronous reference frame and the α-axis in the stationary reference frame are coincident. However, due to a large static friction force and the Stribeck effect, the mover can be slightly misaligned from the ideal point. In that case, by applying an adequate amount of α-axis current, the mover can be rearranged to the desired position, as depicted in Fig. 9. When the mover is at a slightly positive position as in case (a), supplied sufficient positive α-axis voltage can be decomposed into positive d-axis voltage and negative q-axis voltage. The latter induces a negative q-axis current that makes the mover rotate clockwise, until the decomposed component for the q-axis becomes zero (i.e., until the α-axis and the d-axis are coincident). Similarly, in case (c), with the identical positive α-axis voltage as in case (a), the positive q-axis current is induced; then, the mover rotates in a counterclockwise direction, until it reaches the position of case (b). Fig. 10 shows the performance of the proposed method. Compared to Fig. 10(a) without α-axis voltage (V_{alpha}) application (i.e., aligning only with the eye looking), much more accurate initial position is guaranteed with V_{alpha} application, of which the standard deviation in position is about 21.2 μm.

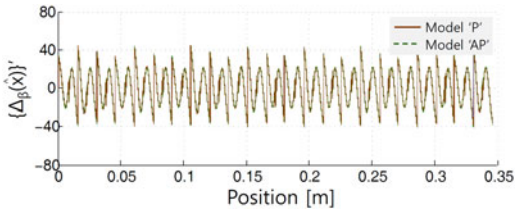

Fig. 11. Differentiation of Δ_β along the position.

TABLE V
SOLO EFFECTS ON POSITION ESTIMATION ERROR IN ARCTAN METHOD

	RMS error		Max. error	
	[mm]	[°E]	[mm]	[°E]
Offset[1]				
0.8%	0.084	0.67	0.120	0.96
1.6%	0.170	1.36	0.240	1.92
Scale[2]				
1%	0.028	0.23	0.040	0.32
2%	0.049	0.39	0.070	0.56
3%	0.078	0.63	0.110	0.88
Phase[3]				
1°E	0.042	0.34	0.060	0.48
2°E	0.092	0.74	0.130	1.04
3°E	0.134	1.07	0.190	1.52
4°E	0.177	1.42	0.250	2.00

[1]Offset, which exists in one of both sine and cosine signals, and normalized to the signal magnitude.[2]Difference in scale between sine and cosine signals, and normalized to the signal magnitude.[3]Undesired phase difference between sine and cosine signals from 90°E due to misalignment.

TABLE VI
MIXED EFFECT ANALYSIS ON POSITION ESTIMATION ERROR IN ARCTANGENT METHOD

Offset	Scale	Phase	RMS error		Max. error	
			[mm]	[°E]	[mm]	[°E]
0.8%	1%	1°E	0.098	0.78	0.190	1.52
1.6%	2%	2°E	0.196	1.57	0.370	2.96
1.6%	3%	3°E	0.227	1.82	0.440	3.52
1.6%	2%	4°E	0.249	1.99	0.490	3.92

B. Fixed Point Iteration Method

In the previous section, Theorem V.1 is regarded as being satisfied. However, since Theorem V.1 itself is presented in a

TABLE VII
POSITION ESTIMATION ERROR CONSIDERING HIGHER ORDER HARMONICS IN ARCTANGENT METHOD

Harmonics order and its magnitude					RMS error		Max. error	
		Second harmonics	Third harmonics	Fourth harmonics	[mm]	[°E]	[mm]	[°E]
Original magnitude	100%	0.6*0.04	0.6*0.10	0.6*0.03	0.69	5.5	1.35	10.8
w/o Third harmonics		0.6*0.04	–	0.6*0.03	0.41	3.3	0.62	5.0
Magnitude ratio to original itself	5%	0.6*0.04*0.05	0.6*0.10*0.05	0.6*0.03*0.05	0.21	1.7	0.41	3.3
	10%	0.6*0.04*0.10	0.6*0.10*0.10	0.6*0.03*0.10	0.23	1.9	0.44	3.5
	20%	0.6*0.04*0.20	0.6*0.10*0.20	0.6*0.03*0.20	0.28	2.2	0.52	4.2
Magnitude ratio to fundamental harmonic	1%	0.6*0.01	0.6*0.01	0.6*0.01	0.26	2.1	0.47	3.8
	2%	0.6*0.02	0.6*0.02	0.6*0.02	0.34	2.7	0.62	5.0
	3%	0.6*0.03	0.6*0.03	0.6*0.03	0.42	3.4	0.79	6.3

[1] In unit of 2500 Gauss.

qualitative expression without any specific figure, the fixed point iteration method is also prepared to support the convergence of the suggested position estimation method.

The fixed point iteration method aims to find approximate solutions of the equation $x = g(x)$ by the numerical method as follows:

$$\hat{x}_n = g(\hat{x}_{n-1}). \tag{4}$$

By defining

$$g(\hat{x}_{n-1}) \triangleq \hat{x}_{n-1} - \frac{y(\hat{x}_{n-1}) - y_m(x_n)}{\beta} \tag{5}$$

the suggested position estimator can be easily formulated in the form of the fixed point iteration method. The convergence property depends on the maximum absolute gradient of the function $g(x)$ and starting point x_0, as stated in the following theorem.

Theorem V.2: Let $g : [a, b] \to [a, b]$ *be a differentiable function such that*

$$|g'(x)| \leq \alpha < 1 \quad for \quad all\ x \in [a, b].$$

Then, the function g *has exactly one fixed point* l_0 *in* $[a, b]$ *and the sequence* (x_n) *with a starting point* $x_0 \in [a, b]$, *converges to* l_0.

Considering the error between the Hall sensor model $y(\hat{x})$ and the linear model, which is the product of the constant inclination angle β and position x in the concerned region, the following equation is definable for the uncertainty defined as Δ_β:

$$y(\hat{x}) \triangleq \beta\hat{x} + \Delta_\beta(\hat{x}). \tag{6}$$

Now, $|g'(x)|$ is calculated as follows:

$$\frac{dg(\hat{x})}{d\hat{x}} = -\frac{\{\Delta_\beta(\hat{x})\}'}{\beta}. \tag{7}$$

The details of derivation are attached in the Appendix. Since $|\beta| \approx 100$ and $|\{\Delta_\beta(\hat{x})\}'| < 50$, as shown in Fig. 11, $|g'(\hat{x})|$ satisfies

$$|g'(\hat{x})| \leq 0.5 < 1. \tag{8}$$

Therefore, the convergence property of the suggested position estimation method is verified.

VI. COMPARATIVE STUDY

For fairness, the square wave Hall sensor with a coarse resolution is not considered. As mentioned earlier, existing studies using linear Hall sensors are adopting the arctangent method for sine and cosine signals. However, such a pair of ideal sinusoid signals (i.e., sine and cosine signals) are not obtainable from sensor measurement signals due to their different intersensor offsets, scales, undesired phase shifts, harmonics, and intermagnet pitch variations. Many studies focused on signal conditioning to eliminate those components. Nevertheless, from a practical point of view, complete compensation of them is almost impossible and there is always a certain amount of impurities in the final refined signals. Therefore, in this section, instead of applying some other signal conditioning methods individually and comparing the performances, an analysis of the influence of still existing unwanted components to the result of the arctangent method is conducted by simulations.

First, the solo influence of offset, scale, and phase on the position estimation error in the arctangent method is summarized in Table V. All the detailed resulting figures are omitted here. The case for coexisting is also given in Table VI.

Adding to the second combination in Table VI, some higher order harmonics are considered. It was confirmed earlier that there are some higher order harmonics in the magnetic flux distribution along the position (Table III). With reference to that, the second-, third-, and fourth-order harmonics are injected with various magnitudes, as shown in Table VII. Since many studies took only the third-order harmonics into account, a special case with completely compensated third-order harmonics but still retaining the second- and fourth-order harmonics is prepared in the second condition in the table. In addition, for the cases in which higher order harmonics are only partially compensated, simulations are conducted with two types of scenarios: the simulation where the amount of uncompensated harmonics remains by the given percentage of the original magnitude and another where it remains by the given percentage of the fundamental harmonic magnitude. All the presented comparative results have much larger errors than that of the suggested method, even though the simulation conditions have fewer "impurities" than the real magnitude in the motor system used in this study.

Furthermore, in the real system, there are inevitable effects like unequally magnetized magnitudes and sizes and intervals between the permanent magnets, as shown in Table III. (This effect was not applied in the simulation results shown in Table VII.) This uneven pole pitch and the variation would appear directly in the arctangent method as an additional estimation error, and the fore position error would be aperiodically integrated to the latter, especially in the case of a linear motor system.

VII. Conclusion

In this paper, a new position estimator was designed using three linear Hall sensors for a permanent magnet linear motor system. Other existing studies, which use linear Hall sensors for the position estimation, instead of high priced encoders and resolvers, utilize the arctangent method with sensor measurement signals after signal conditioning. However, from a practical point of view, the signal is quite not in a sinusoidal form, especially in a linear motor system in which the sensor offset, scale difference, unwanted phase shift, higher order harmonics, and uneven pole pitch effects are significant. Hence, a new method is suggested in the following procedures: First, the sensor signal is modeled along the position as a polynomial of harmonics functions through FFT without any low-pass filter for noise rejection or additional signal conditioning. Then, after initial position aligning, a fixed point iteration method is used to estimate the position. This strategy takes the full advantage of Hall sensor properties, which have robust characteristics to the environmental contamination such as water, oil, dust, and external disturbances like vibrations and shocks. Furthermore, even though the sensor measurement is sensitive to temperature change, it is not an issue in a linear motor system due to its open structure. The armature reaction is also negligible. Finally, the convergence of the suggested iterative method was proved mathematically, and the performance of the designed estimator was verified using very low cost production Hall sensors and a prototype linear motor system. The performance analysis confirmed that this method is suitable for applications requiring precision and accuracy to a few electrical degrees as well as a long travel range. However, the magnetic flux density itself can change according to overheating of the permanent magnet and that is an issue to be addressed in the future.

Appendix

This appendix provides the details of derivation of (7).

$$\begin{aligned}\frac{dg(\hat{x})}{d\hat{x}} &= \frac{d\left\{\hat{x}-\frac{y(\hat{x})-y_m}{\beta}\right\}}{d\hat{x}} \\ &= 1-\frac{1}{\beta}\left\{\frac{dy(\hat{x})}{d\hat{x}}\right\} \\ &= 1-\frac{1}{\beta}\left[\frac{d\left\{\beta\hat{x}+\Delta_\beta(\hat{x})\right\}}{d\hat{x}}\right] \\ &= -\frac{\{\Delta_\beta(\hat{x})\}'}{\beta}.\end{aligned}$$

References

[1] J. Kim, K. Cho, and S. Choi, "Lumped disturbance compensation using extended Kalman Filter for permanent magnet linear motor system," *Int. J. Control Autom. Syst.*, to be published, doi: 10.1007/s12555-014-0400-1.

[2] K. Cho, J. Kim, S. Choi, and S. Oh, "A high-precision motion control based on a periodic adaptive disturbance observer in a PMLSM," *IEEE/ASME Trans. Mechatronics*, vol. 20, no. 5, pp. 2158–2171, Oct. 2015.

[3] S. Sarma, V. K. Agrawal, and S. Udupa, "Software-based resolver-to-digital conversion using a DSP," *IEEE Trans. Ind. Electron.*, vol. 55, no. 1, pp. 371–379, Jan. 2008.

[4] C. Yim, I. Ha, and M. Ko, "A resolver to digital conversion method for fast tracking," *IEEE Trans. Ind. Electron.*, vol. 39, no. 5, pp. 369–378, Oct. 1992.

[5] N. Matsui, "Sensorless PM brushless DC motor drives," *IEEE Trans. Ind. Electron.*, vol. 43, no. 2, pp. 300–308, Apr. 1996.

[6] Y. Jung and M. Kim, "Sliding mode observer for sensorless control of IPMSM drives," *KIPE J. Power Electron.*, vol. 9, no. 1, pp. 117–123, Jan. 2009.

[7] L. I. Iepure, I. Boldea, and F. Blaabjerg, "Hybrid I-f Starting and observer-based sensorless control of single-phase BLDC-PM motor drives," *IEEE Trans. Ind. Electron.*, vol. 59, no. 9, pp. 3436–3444, Sep. 2012.

[8] S. Shinnaka, "New D-state-observer-based vector control for sensorless drive of permanent-magnet synchronous motors," *IEEE Trans. Ind. Appl.*, vol. 41, no. 3, pp. 825–833, May/Jun. 2005.

[9] H. A. Toliyat, L. Hao, D. S. Shet, and T. A. Nondahl, "Position-sensorless control of surface-mount permanent-magnet AC (PMAC) motors at low speeds," *IEEE Trans. Ind. Electron.*, vol. 49, no. 1, pp. 157–164, Feb. 2002.

[10] A. Accetta, M. Cirrincione, M. Pucci, and G. Vitale, "Sensorless control of PMSM fractional horsepower drives by signal injection and neural adaptive-band filtering," *IEEE Trans. Ind. Electron.*, vol. 59, no. 3, pp. 1355–1366, Mar. 2012.

[11] Y. Inoue, Y. Kawaguchi, S. Morimoto, and M. Sanada, "Performance improvement of sensorless IPMSM drives in a low-speed region using online parameter identification," *IEEE Trans. Ind. Appl.*, vol. 47, no. 2, pp. 798–804, Mar./Apr. 2011.

[12] S. Yang, K. Cho, and C. Hong, "Sensorless control of a permanent magnet synchronous motor with compensation of the parameter variation," (in Korean), in *Proc. KIPE*, Dec. 2002, vol. 7, no. 6, pp. 517–523.

[13] S. Kim, C. Choi, K. Lee, and W. Lee, "An improved rotor position estimation with vector-tracking observer in PMSM drives with low-resolution Hall-effect sensors," *IEEE Trans. Ind. Electron.*, vol. 58, no. 9, pp. 4078–4086, Sep. 2011.

[14] C. Choi, K. Lee, and W. Lee, "Observer-based phase-shift fault detection using adaptive threshold for rotor position sensor of permanent-magnet synchronous machine drives in electromechanical brake," *IEEE Trans. Ind. Electron.*, vol. 62, no. 3, pp. 1964–1974, Mar. 2015.

[15] I. Boldea, M. C. Paicu, and G. D. Andreescu, "Active flux concept for motion-sensorless unified AC drives," *IEEE Trans. Power Electron.*, vol. 23, no. 5, pp. 2612–2618, Sep. 2008.

[16] G. Foo and M. F. Rahman, "Sensorless direct torque and flux-controlled IPM synchronous motor drive at very low speed without signal injection," *IEEE Trans. Ind. Electron.*, vol. 57, no. 1, pp. 395–403, Jan. 2010.

[17] K. Cho, Y. Lee, H. Mok, H. Kim, B. Jun, and Y. Cho, "Torque ripple reduction of a PM synchronous motor for electric power steering using a low resolution position sensor," *KIPE J. Power Electron.*, vol. 10, no. 6, pp. 709–716, Nov. 2010.

[18] Y. Liu, J. Zhao, M. Xia, and H. Luo, "Model reference adaptive control-based speed control of brushless DC motors with low-resolution Hall-effect sensors," *IEEE Trans. Power Electron.*, vol. 29, no. 3, pp. 1514–1522, Mar. 2014.

[19] Y. Yang and Y. Ting, "Improved angular displacement estimation based on Hall-effect sensors for driving a brushless permanent-magnet motor," *IEEE Trans. Ind. Electron.*, vol. 61, no. 1, pp. 504–511, Jan. 2014.

[20] G. Jing, O. Minggao, L. Jianqiu, L. Dongbin, F. Chuan, and M. Yan, "Driving and braking control of PM synchronous motor based on low-resolution Hall sensor for battery electric vehicle," *Chin. J. Mech. Eng.*, vol. 26, no. 1, pp. 1–10, 2013.

[21] P. Alaeinovin and J. Jatskevich, "Filtering of Hall-sensor signals for improved operation of brushless DC motors," *IEEE Trans. Energy Convers.*, vol. 27, no. 2, pp. 547–549, Jun. 2012.

[22] A. Yoo, S. Sul, D. Lee, and C. Jun, "Novel speed and rotor position estimation strategy using a dual observer for low-resolution position sensors," *IEEE Trans. Power Electron.*, vol. 24, no. 12, pp. 2897–2906, Dec. 2009.

[23] Z. M. Dalala, Y. Cho, and J. Lai, "Enhanced vector tracking observer for rotor position estimation for PMSM drives with low resolution Hall-effect position sensors," in *Proc. IEEE Elect. Mach., Drives Conf.*, 2013, pp. 484–491.
[24] K. K. Tan, P. V. Er, R. Yang, and C. S. Teo, "Selective precision motion control using weighted sensor fusion approach," in *Proc. IEEE Int. Conf. Mechatronics Autom.*, 2013, pp. 179–184.
[25] L. Baghli and B. Khouane, "Position estimation of linear synchronous motor using Hall-effect sensors and a MEMS accelerometer," in *Proc. IEEE Int. Conf. Syst. Control*, 2013, pp. 989–994.
[26] Y. Y. Lee, R. H. Wu, and S. T. Xu, "Applications of linear Hall-effect sensors on angular measurement," in *Proc. IEEE Int. Conf. Control Appl.*, 2011, pp. 479–482.
[27] H. Ahn and K. Kim, "2D Hall sensor array for measuring the position of a magnet matrix," *Int. J. Precision Eng. Manuf. Green Technol.*, vol. 1, no. 2, pp. 125–129, Apr. 2014.
[28] S. Jung and K. Nam, "PMSM control based on edge-field Hall sensor signals through ANF-PLL processing," *IEEE Trans. Ind. Electron.*, vol. 58, no. 11, pp. 5121–5129, Nov. 2011.
[29] J. Hu, J. Zou, F. Xu, Y. Li, and Y. Fu, "An improved PMSM rotor position sensor based on linear Hall sensors," *IEEE Trans. Magn.*, vol. 48, no. 11, pp. 3591–3594, Nov. 2012.
[30] Z. Q. Zhu, Y. F. Shi, and D. Howe, "Rotor position sensing in brushless ac motors with self shielding magnets using linear Hall sensors," *J. Appl. Phys.*, vol. 99, Apr. 2006, Art. no. 08R313.
[31] K. J. Meessen, B. L. J. Gysen, J. J. H. Paulides, and E. A. Lomonova, "Three-dimensional magnetic field modeling of a cylindrical Halbach array," *IEEE Trans. Magn.*, vol. 46, no. 6, pp. 1733–1736, Jun. 2010.
[32] B. L. J. Gysen, K. J. Meessen, J. J. H. Paulides, and E. A. Lomonova, "Semi-analytical calculation of the armature reaction in slotted tubular permanent magnet actuators," *IEEE Trans. Magn.*, vol. 44, no. 11, pp. 3213–3216, Nov. 2008.
[33] K. J. Meessen, J. J. H. Paulides, and E. A. Lomonova, "Modeling and experimental verification of a tubular actuator for 20-g acceleration in a pick-and-place application," *IEEE Trans. Ind. Appl.*, vol. 46, no. 5, pp. 1891–1898, Sep./Oct. 2010.
[34] J. W. Jansen, J. P. C. Smeets, T. T. Overboom, J. M. M. Rovers, and E. A. Lomonova, "Overview of analytical models for the design of linear and planar motors," *IEEE Trans. Magn.*, vol. 50, no. 11, Nov. 2014, Art. no. 8206207.

Jonghwa Kim (S'16) received the B.S. degree in materials engineering from Hokkaido University, Sapporo, Japan, in 2006, and the M.S. degree in mechanical engineering from Korea Advanced Institute of Science and Technology, Daejeon, South Korea, in 2009, where he is currently working toward the Ph.D. degree in mechanical engineering.

From 2009 to 2012, he was an Assistant Research Engineer with the Welding R&D Center, STX Offshore&Shipbuilding Co., Ltd., South Korea. His research interests include state estimation, high accuracy and precision motion control in linear motor systems.

Seibum Choi (M'08) received the B.S. degree in mechanical engineering from Seoul National University, Seoul, South Korea, in 1985, the M.S. degree in mechanical engineering from Korea Advanced Institute of Science and Technology (KAIST), Daejeon, South Korea, in 1987, and the Ph.D. degree in controls from the University of California, Berkeley, CA, USA, in 1993.

From 1993 to 1997, he was with the Institute of Transportation Studies, University of California, working on the development of automated vehicle control systems. Through 2006, he was with TRW, Livonia, MI, USA, where he worked on the development of advanced vehicle control systems. Since 2006, he has been with the faculty of the Mechanical Engineering Department, KAIST. His research interests include fuel-saving technology, vehicle dynamics and control, and active safety systems.

Prof. Choi is a Member of the American Society of Mechanical Engineers, the Society of Automotive Engineers, and the Korean Society of Automotive Engineers.

Kwanghyun Cho (S'11–M'16) received the B.S. degree in electrical engineering and computer science from Kyungpook National University, Daegu, South Korea, in 2008, and the M.S. and Ph.D. degrees in mechanical engineering from Korea Advanced Institute of Science and Technology, Daejeon, South Korea, in 2010 and 2014, respectively.

He is currently a Senior Engineer in the Mechatronics R&D Center, Samsung Electronics Co., Ltd., Hwaseong-si, South Korea. His research interests include precision motion control based on linear motors.

Kanghyun Nam (S'10–M'12) received the B.S. degree in mechanical engineering from Kyungpook National University, Daegu, South Korea, in 2007, the M.S. degree in mechanical engineering from Korea Advanced Institute of Science and Technology, Daejeon, South Korea, in 2009, and the Ph.D. degree in electrical engineering from The University of Tokyo, Tokyo, Japan, in 2012.

From 2012 to 2015, he was a Senior Engineer with Samsung Electronics Co., Ltd., Gyeonggi-do, South Korea. Since 2015, he has been an Assistant Professor in the School of Mechanical Engineering, Yeungnam University, Gyeongsan, South Korea. His research interests include motion control, vehicle dynamics and control, electric vehicles, and industrial mechatronics.

Prof. Nam is a Member of the Society of Automotive Engineers of Japan and the Korean Society of Automotive Engineers. He received the Best Paper Award from the IEEE TRANSACTIONS ON INDUSTRIAL ELECTRONICS in 2014.